AN INTEGRATED GEOPHYSICAL STUDY OF THE LITHOSPHERIC STRUCTURE BENEATH LIBYA

Wesley A. Brown, Thomas F. VanDeMark, Diane I. Doser, and Aaron A. Velasco

University of Texas at El Paso

Sponsored by Air Force Research Laboratory

Contract No. DTRA01-01-C-0058

ABSTRACT

We have used over 6,000 gravity measurements, in conjunction with other geophysical and geological data obtained from oil exploration, published research, and other academic institutions to develop a three-dimensional (3-D) density model for the Libya region. Next we derived a preliminary 3-D velocity model (called LIBYA3D) based on this density model. Our resulting 1-D approximation of the 3-D velocity model was found to compare favorably with the standard 1-D IASPEI91 (International Association of Seismology and Physics of the Earth's Interior) velocity model. We verified our velocity model by deriving individual velocity models along specific source receiver paths traversing our study area (1.5-D). Only earthquakes of 4.7m_b or greater occurring in Libya were found to be suitable sources for this analysis. Our velocity models were then used to generate synthetic waveforms for waveform modeling. Analysis of the preliminary results from the waveform modeling indicates that our 1-D velocity model is valid for frequencies greater than 20 s. We are confident that our velocity model of subsurface Libya has improved our understanding of the regional wave propagation and will be useful to the nuclear testing community and to anyone interested in a better understanding of the seismicity of the area.

We also utilize this model in the context of regional discrimination to investigate small to moderate size natural events (m_b 3.7 – 5.7) in the Libyan region occurring from May 1990 to May 2000. Observations of Pn and Sn energy at varying frequency ranges (0.5 – 8 Hz) and propagation paths recorded by broadband instrumentation lead us to investigate the attenuation affects the geologic structure of the Libyan region and the adjacent Mediterranean Sea. We perform multi-frequency analysis to discern which frequencies have the optimum signal-to-noise ratio (SNR) for these regional phases. Pn and Sn show stronger amplitudes at higher frequencies (4 – 8 Hz) along propagation paths where continental crust is limited. Conversely, we only observe strong Pn and Sn amplitudes at lower frequencies (0.5 – 4 Hz) along propagation paths where continental crust is prevalent. We utilize LIBYA3D to develop trends in our data as a function of crustal path and volume. These empirical observations could be used to aid future clandestine explosion discrimination work in the Libyan region if the need arises.

OBJECTIVE

To monitor a zero yield nuclear explosion treaty, we must be able to analyze events of all magnitudes that occur throughout the world. Furthermore, it is difficult to analyze the effectiveness of discriminating between earthquakes and explosions when there are a small amount of events to analyze. Compounding problems arise with small magnitude events recorded at regional distances, since path effects can lead to complex regional seismograms causing misclassification of events (e.g., Velasco et al., 2003). The Libyan region exhibits many of these difficulties, where there are few events, and those that occur are generally small in magnitude. One approach to overcome some of these difficulties is to develop velocity models utilizing auxiliary data, and build a model from which we can build confidence in discrimination at regional distances. We develop a 3-D velocity/density model (LIBYA3D) of a portion of subsurface Libya from over 6,000 gravity data points available for the region. We validate the model with regional waveforms, and then apply this model for a discrimination analysis in the region.

RESEARCH ACCOMPLISHED

3-D Model Development & Validation

Our model consists of five lithospheric layers and an extra layer accounting for the Mediterranean Sea is added as necessary. We calculated the dimensions of the Mediterranean Sea within the study area by writing a small Microsoft excel script that assigns an elevation of 0 km depth to areas of the DEM with elevation less than 0 km. The difference between the newly calculated body (i.e. Mediterranean body excluded) and the original DEM defines the expanse of the Mediterranean Sea. The standard density of sea water 1.1g/cc was assigned to this water layer. The Cenozoic and Mesozoic units were treated as a single layer. The base of the Mesozoic and the top of the Precambrian Basement were digitized from a 1:2,000,000 structure contour map of the Libyan Arab Republic and adjacent areas; compiled by G. H. Goudarzi, U.S. Geological Survey with J. P. Smith as consulting Geologist, 1978. Both sets of contours were drawn at intervals of 250m. The top of the Precambrian Basement and the bottom of the Mesozoic layer sandwiches the Paleozoic layer which is assigned a density of 2.55g/cc. The top of the lower crust was set at a depth of 19 km (Dial 1998) and the surface of the Moho was digitized from Dial (1998). The various densities assigned were obtained from Dial 1998 and Carmichael 1989. We call our model “LIBYA3D”.

Resulting 3-D velocity model

Figure 1 is the average velocity/density model resulting from the study compared to the standard IASPEI91 model. The velocities used in this model were derived using the Nafe-Drake method in conjunction with previous studies from Dial (1998). Overall the resulting velocity/density model showed a good correlation with the IASPEI91 model in all three quantities. The values for the *P*-wave and *S*- wave velocities for the IASPEI91 model are generally slightly too low for subsurface Libya. For the Moho both models returned identical values for *P*- and *S*-wave velocities; however, a density of 3.3 g/cc was assigned to our model as opposed to 3.396 g/cc in the IASPEI91 model. Again our LIBYA3D model consistently showed slightly higher values than the IASPEI91 for density. The widest margin of disparity occurred within the lower crust where the *P*-wave velocity estimation for the lower crust according to the IASPEI91 model is 6.5 km/s while other studies (Seber et al 1996, McNamara et al. 1996) showed that a higher *P*-wave velocity exists. Dial’s study led him to conclude that a value of 7.16 is the most reliable *P*-wave velocity for the lower crust in the region. For the Precambrian layer the general trend remained the same, slightly too low on the part of the IASPEI91 model. Above the Precambrian basement layer the IASPEI91 model did not differentiate for any of the divisions and assigned a uniform value of 5.8 km/s, 3.46 km/s, and 2.449g/cc to the *P*-wave velocity, *S*-wave velocity and density, respectively. For our model however, having digitized the surface of the top of the Precambrian Basement rock and the base of the Mesozoic surface, we were able to assign values to each. The top of the lower crust is set to a depth of 19 km in our model instead of 20 km as in the IASPEI91 model, since there are better regional seismic constrains in the area. In the Libya region, the crust thins towards the north and so it is inaccurate to assign a single value for the depth to the Moho. Since we have a 1-D model, we used the average value of 35 km (Figure 2), which is the same as the value used in the IASPEI91 model. The small overall differences between the IASPEI91 model and our LIBYA3D model may be subtle, but on a localized scale, we can expect to see a difference in the effect on seismic waves.

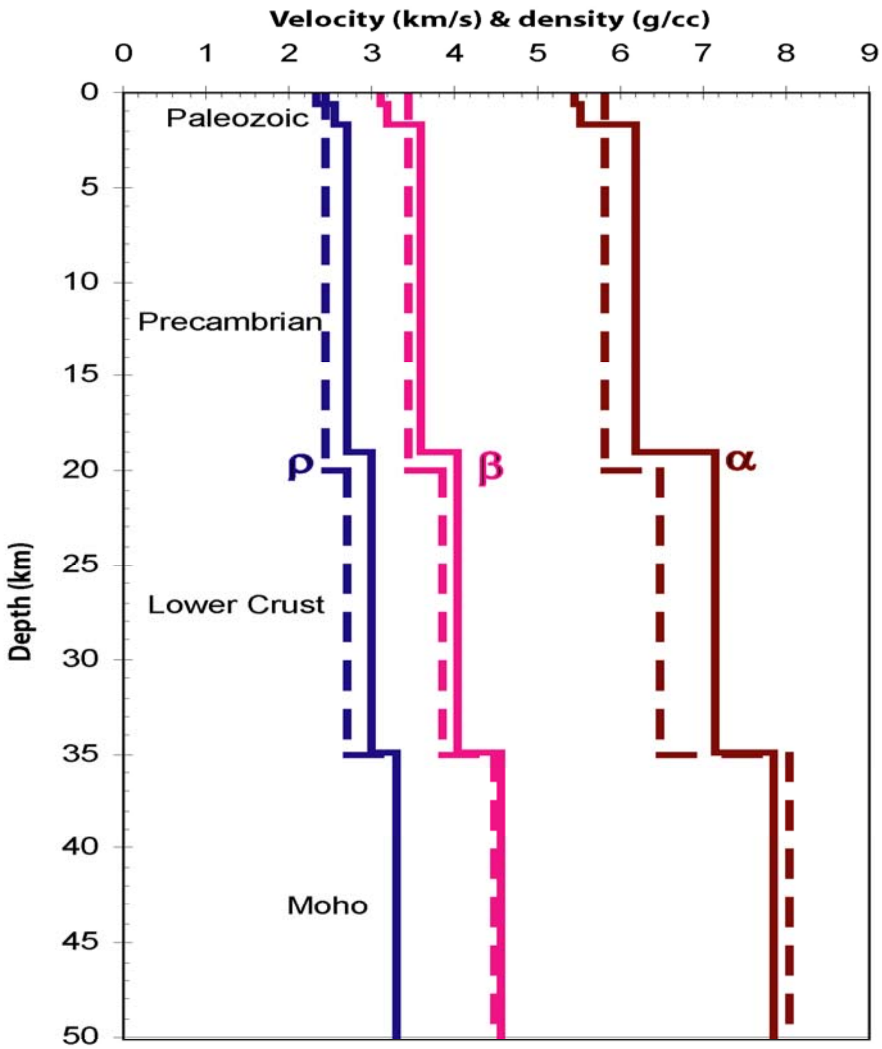

Figure 1: Velocity/density model as derived from our investigation compared with the standard IASPEI91 global velocity model. The broken lines represent the IASPEI91 model and the solid lines show results from our model. Blue lines show density values, magenta lines show S-wave velocity values, and the brown lines show the P-wave velocity values.

Validation of 3-D Velocity Model

We carried out a preliminary seismic evaluation on the average 1-D velocity model. Event 910808 (YYMMDD) is of magnitude 4.7m_b located at 35.65N and 11.64E and was chosen since it sampled a significant portion of the study area and a part of the Mediterranean Sea. The waveform collected for this event was also good enough for seismic analysis to be carried out. We computed a predicted travel time for the event to station KEG in Egypt using our 1-D model and compared the results to the actual waveform recorded in KEG and visually inspect for a match. The results were satisfactory.

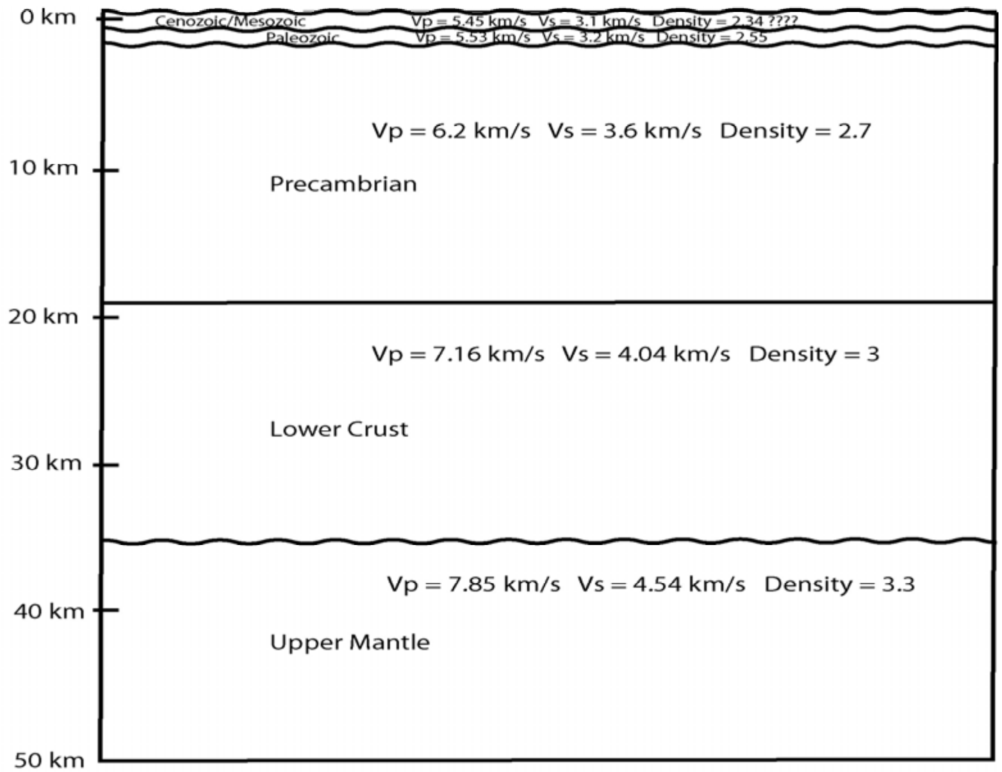

Figure 2: Shows the average 1-D velocity and density model beneath Libya. The wavy lines show surfaces that were digitized from data. A uniform depth of 19 km was assumed for the top of the lower crust.

Next we calculated individual path specific velocity models for two other events in order to do a 1.5D velocity model. Events 980528 and 921012 (Figure 3, Table 1) were chosen as the source-receiver path traversed the Libyan lithosphere and was not greatly affected by lithospheric structure at distances beyond the study area. Special care had to be taken when choosing source-receiver pathways since the border between the African plate and the Eurasian plate is situated to the north of Libya. In this area there is considerable thinning of the crust and a velocity gradient exists.

An unfiltered seismogram of event 910808 (Figure 4) is tested against the averaged 1-D model. The red line shows the predicted P-wave arrival time (T_0) for the event generated from our model. We used SAC to carry out the seismic analysis for this portion of the study. The predicted arrival time accurately coincides with the arrival time of the *P*-wave. Other similar tests carried out further validated our 1-D model. The preliminary results of the modeling of the two events are shown in Figure 5. The seismograms are filtered using a low pass Butterworth filter of 0.05Hz. For event 921012 we observed a close correlation between the synthetic and the recorded seismogram on the vertical and transverse components while we did not receive a good fit on the radial component. For event 980528 we again observed favorable correlation on the vertical component but were off on the radial and transverse components. This could be due to the presence of sedimentary basins that are not accounted for.

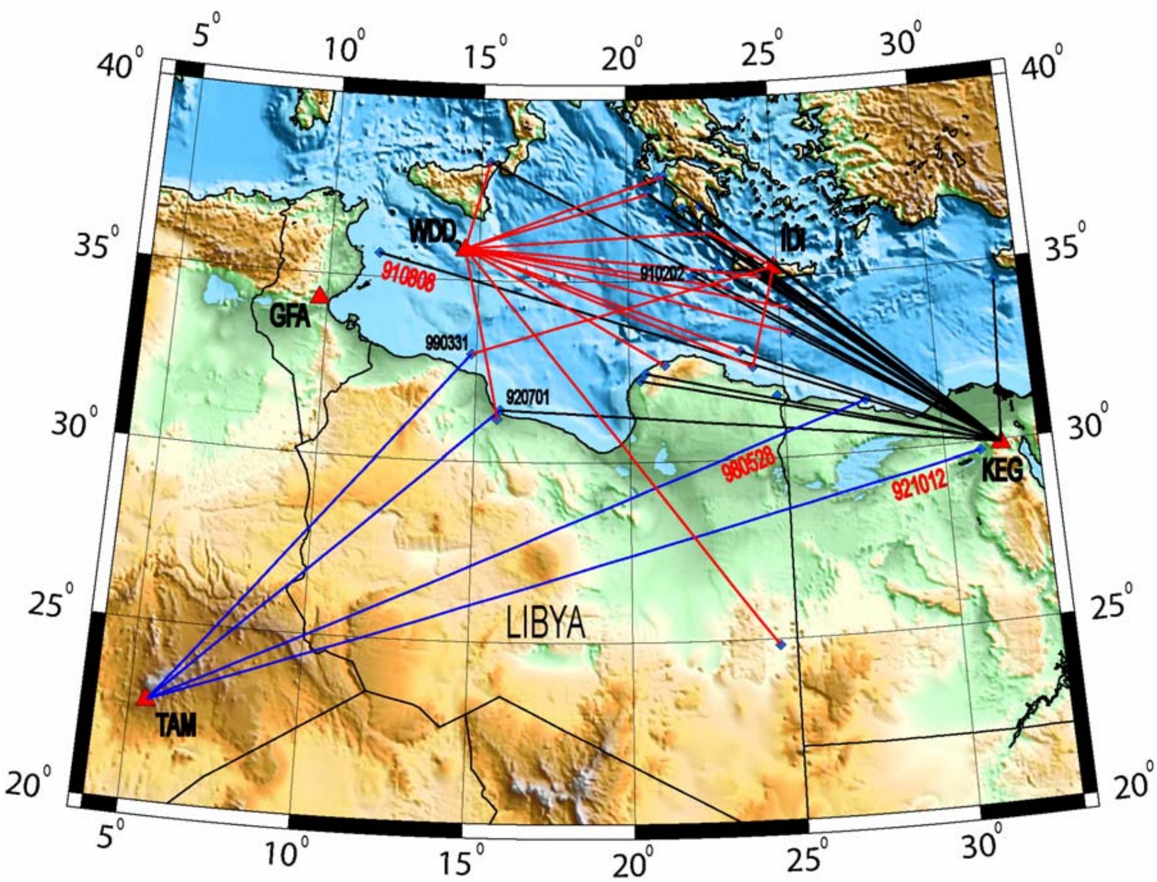

Figure 3: Map of study shows earthquakes as blue diamonds, stations as red triangles, and multi-colored great circle arcs represent source-receiver paths.

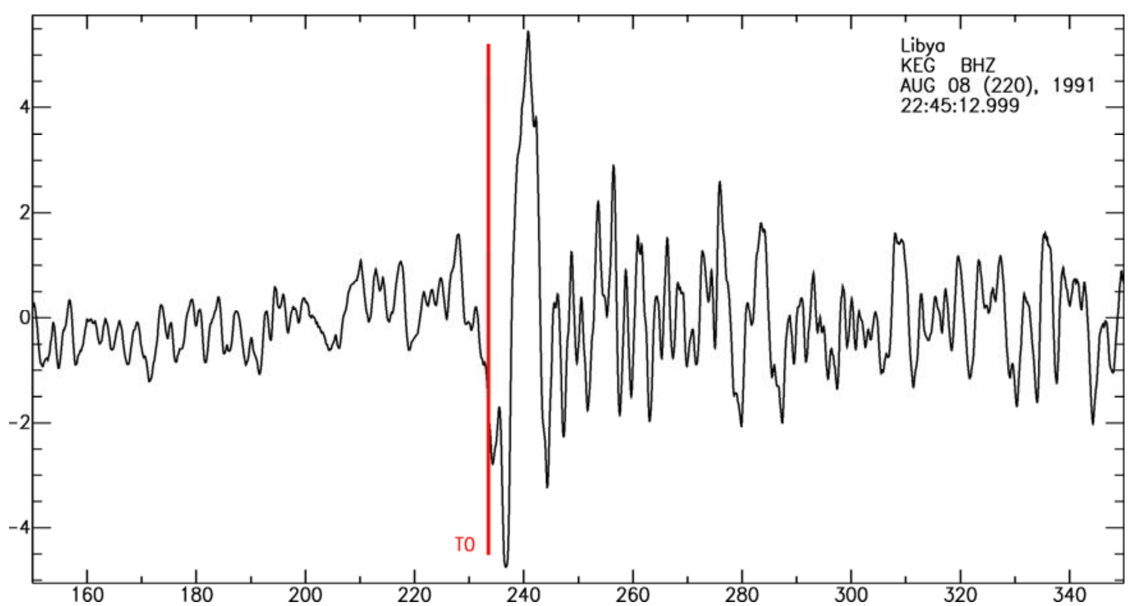

Figure 4: Unfiltered seismogram of event 910808. The red line (T0) shows the predicted *P*-wave arrival time using our derived model.

Table 1: List of earthquakes used for research project. Times and locations are provided by the International Seismic Centre (ISC).

Date	Time	Lat.	Lon.	Depth	Mag.
2000/05/21	22:45:38.3	31.1570	15.7340	23.6	mb 3.8
1990/05/18	18:27:51.2	31.7130	24.7960	10.0	MD 4.3
1990/05/25	15:44:45.9	37.8702	21.0578	1.0	mb 3.8
1990/07/30	17:52:37.9	34.4845	25.5438	45.8	mb 4.4
1991/02/02	05:34:47.3	35.1190	22.1571	10.0	mb 3.7
1991/02/08	13:50:40.1	35.2852	23.0458	63.8	mb 4.4
1991/05/28	18:58:46.6	37.0235	22.4817	20.8	mb 4.5
1991/08/08	22:46:10.9	35.6467	11.6387	22.0	mb 4.7
1992/07/01	15:13:32.8	31.4246	15.8143	10.0	mb 4.2
1992/10/12	13:09:55.4	29.7566	31.1360	21.5	mb 5.8
1993/09/09	00:32:35.5	32.2394	20.3859	10.0	mb 4.8
1995/07/22	06:24:45.5	34.7502	23.3754	72.2	mb 4.1
1995/08/02	01:42:20.6	33.4384	25.3153	33.0	mb 3.4
1995/08/27	19:42:14.7	38.2610	15.2912	25.2	mb 3.6
1995/11/25	14:10:46.0	28.8123	34.9227	14.0	mb 3.8
1996/01/06	10:38:23.9	32.9867	23.6555	1.0	
1996/03/23	20:40:46.9	36.9910	21.8653	30.3	mb 3.5
1996/05/19	14:15:14.2	34.1160	25.3398	37.6	mb 4.0
1996/06/21	13:03:38.5	37.8847	21.2394	91.1	mb 3.5
1996/10/09	16:57:40.1	36.8145	21.2931	13.6	mb 4.0
1996/10/09	17:01:49.0	34.4148	32.1809	50.2	mb 4.1
1996/10/30	10:43:02.9	32.4343	20.5326	10.0	mb 4.6
1997/02/01	23:08:36.0	35.0318	24.4391	10.0	mb 3.9
1997/05/10	14:03:03.6	24.8180	24.4750	0.0	mb 3.9
1998/01/13	12:34:21.1	37.3992	20.7101	15.1	mb 3.6
1998/04/12	22:06:31.0	37.4186	20.7159	10.0	mb 4.4
1998/05/28	18:33:28.4	31.4459	27.6426	10.0	mb 5.5
1998/08/08	16:39:28.7	36.2939	22.7695	5.0	mb 3.5
1999/03/31	09:42:16.1	32.9550	14.8380	32.2	mb 4.3
1999/06/17	10:18:02.2	32.5410	24.0530	10.0	mb 4.3
1999/11/07	14:43:36.0	32.6600	21.1740	10.0	mb 4.4

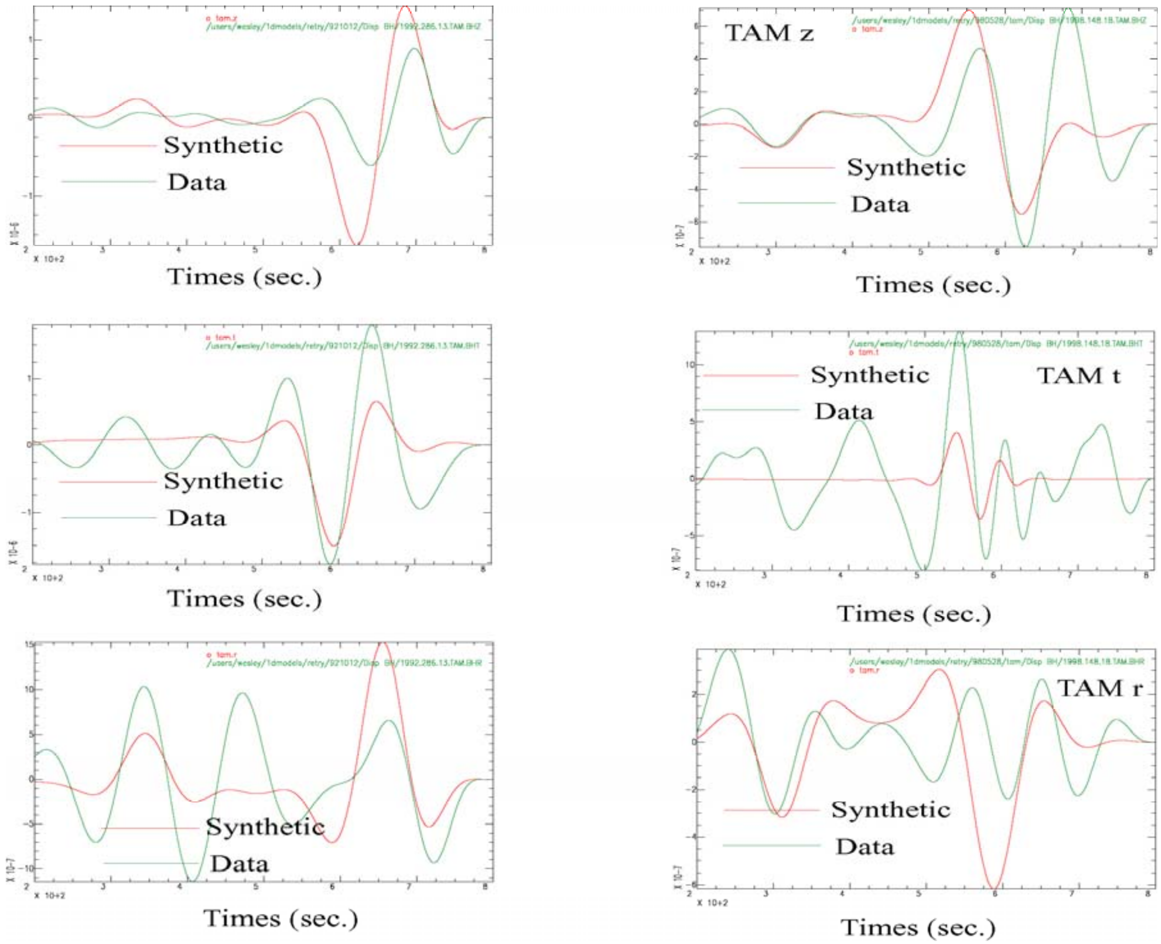

Figure 5: Waveform comparison between synthetic and data for events 980528 and 921012 (Table 1) used in validation study.

Application for Regional Discrimination

We investigate events in and around Libya (Figure 3, Table 1). Problems arise because there is no explosion data for Libya, and we are limited by the small number of reliable stations at regional distances. However, we apply our LIBYA3D model for discrimination purposes. We gather seismic data for events that occurred from 18 May 1990 to 21 May 2000 in the Libyan region and the adjacent Mediterranean Sea. Event times and locations were obtained from the International Seismic Centre (ISC). We have data consisting of 31 natural events, 7 located in Libya, 1 located in Egypt, with the remainder located in the adjacent area of the Mediterranean Sea. Magnitudes range from (m_b) 3.7 to 5.7. The stations used in this research effort are Kottamia, Egypt (KEG), Wield Dalam, Malta (WDD), Tamanrasset, Algeria (TAM), Anoyia, Crete (IDI), and Gafsa, Tunisia (GFA), all with broadband instrumentation (Figure 3). Initial multi-frequency analysis of events (e.g., Walter et al., 1995) showed consistent high frequency propagation of Pn and Sn energy at KEG and low frequency propagation of Pn and Sn energy at TAM. We show the 02 February 1991 (910202) event (see Figure 6) recorded at KEG ($\Delta = 9.67^o$; AZ = 120), which leads us to investigate attenuation affects of source-receiver paths as related to their orientation across the varying topography and bathymetry of Libya and the Mediterranean Sea. We use the 3-D model to investigate path effects associated with signal-to-noise ratio. We also identify path dependent cross spectral ratios (Walter et al., 1995) which show the elevated SNR frequency ranges at specific stations as solid parameters for future verification work.

Two events of particular interest, due to have being recorded at two receivers are the 31 March 1999 (990331) event recorded at IDI ($\Delta = 8.66^o$; AZ = 71.9^o) and TAM ($\Delta = 13.1^o$; AZ = 221^o), and the 01 July 1992 (920701) event recorded at KEG ($\Delta = 13.9^o$; AZ = 92.0^o) and TAM ($\Delta = 12.6^o$; AZ = 229^o) (see Figure 3)

Signal-to-Noise and Amplitude Ratios

Waveform data was acquired from the Incorporated Research Institutions for Seismology's (IRIS) Data Management Center (DMC). We remove instrument response and set origin times for each event. Waveform data is then cut and rotated to its radial and transverse components, and finally, we apply a Butterworth filter to view the waveform at several frequency ranges (0.5-1, 1-2, 2-4, 4-6, and 6-8 Hz) (Figure 6).

We pick regional phases Pn and Sn manually and mark the header for each waveform. We calculate phase amplitude and SNR by measuring the maximum displacement in a ten second pre-phase and phase window. By comparing the SNR of Pn against frequency at a specific station (Figures 7A-C) we observe trends in station-frequency dependence. These trends were normalized by dividing each point by the SNR at the lowest frequency range for each event (0.5-1.0 Hz). This highlights the difference in high frequency propagation. We also calculate cross-spectral ratio values (1-2 / 6-8 Hz) (Walter *et al.,* 1995) by using both displacement and SNR measurements. In this way we can define the events with high-frequency propagation by there low cross-spectral value.

As expected the SNR for both events at TAM is low from 4 to 8 Hz; however at IDI and KEG the SNR is still large if not dominant from 4 to 8 Hz. Note the receiver distance to KEG is greater than the receiver distance to TAM for 920701, but the SNR is still strong enough to be seen at KEG in the high frequency ranges. This shows us that receiver distance is not the primary controlling parameter for signal attenuation. As seen in the SNR-Frequency diagrams, (Figures 7A-C) KEG conveys the most dramatic results with the SNR peaking at 6-8 Hz in 10 of the 14 events recorded there. IDI and WDD show a trend similar to KEG with good SNR at 4 to 8 Hz, but actually peak at 3 Hz for most of these Intra-Mediterranean events. We combine their results due to their similar trends, as well as their receiver environments are the same topographically. TAM shows expected high frequency attenuation of Pn energy.

Using LIBYA3D and a 0.5 degree wide swath, we calculate the crustal volume for each source-receiver path. We also use a simple, but accurate map measurement to determine the percentage of continental crust in each source-receiver path. We also calculate cross-spectral amplitude and cross-spectral SNR values and X-Y diagrams are made by plotting these topographic statistics against the cross-spectral values and correlations are sought (Figures 8A, B) (e.g., Zhang & Lay, 1994). At KEG we find a strong correlation between high frequency propagation and the percentage of continental crust in the source-receiver path when compared to cross-spectral amplitude (Figures 8A, B) and a weak correlation between high frequency propagation and crustal volume. We see similar results for KEG when compared to cross-spectral SNR. There is a correlation for percentage of continental crust, and a weak trend when compared to crustal volume. For IDI, WDD, and TAM there is some correlation when comparing percentage of continental crust and crustal volume to cross-spectral SNR. However, these correlations break down when compared to cross-spectral amplitude.

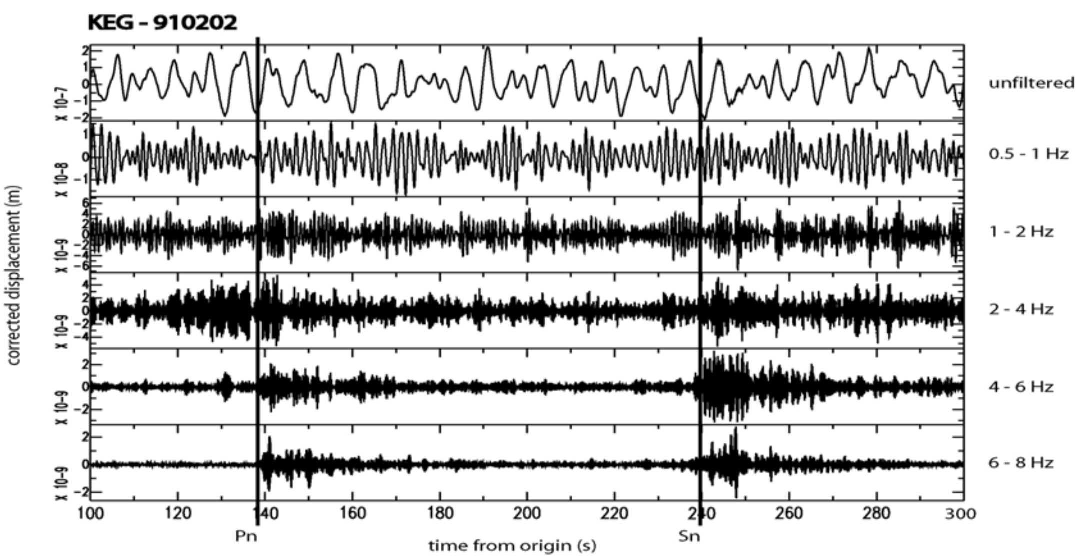

Figure 6: Multi-frequency bandpassed seismogram of the 01 July 1992 event recorded at KEG. Note that SNR increases at the higher frequency ranges. This is a good example that led us to question what path effects were responsible for high frequency propagation such as this.

Finally, we compare cross-spectral values of regional Libyan earthquakes against values of Nevada Test Site (NTS) earthquakes and explosions to show certain frequency ranges at specific stations as solid verification parameters (Figure 9). The figure shows two distinct populations; one of NTS events and one of Libyan events. We note the good separation of the two populations through the entire range of magnitude.

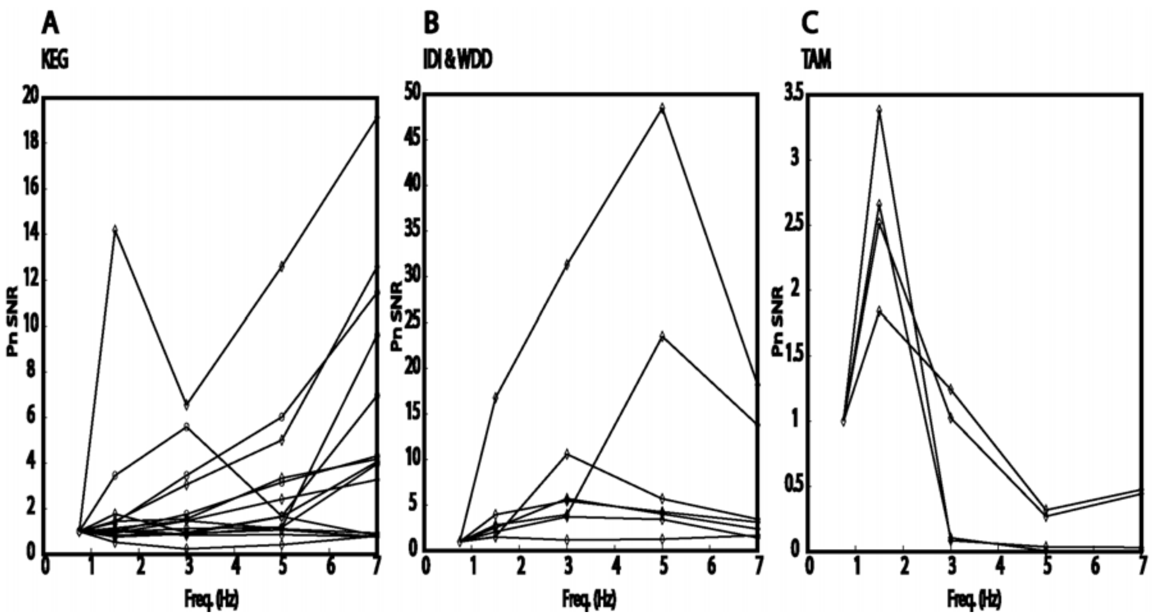

Figure 7: SNR-Frequency diagrams show trends in station-frequency dependence, note the unusual high frequency propagation displayed at KEG accompanied by the expected high frequency attenuation at TAM.

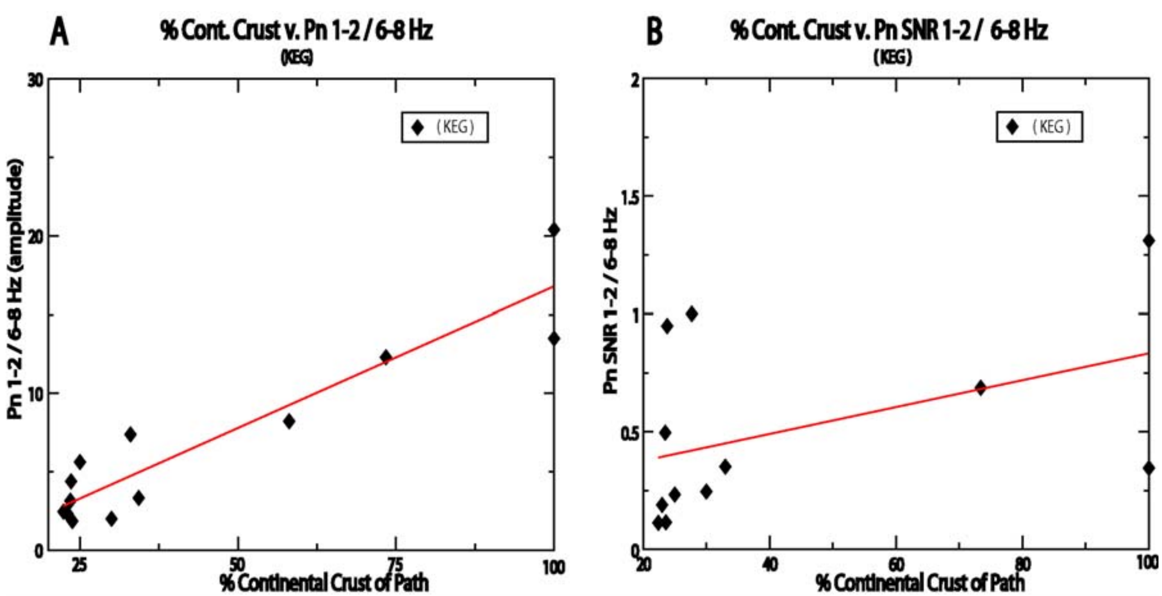

Figure 8: Shows a good correlation between the percentage of continental crust in the source-receiver path and cross-spectral values. Note the lower the cross-spectral value the better the high frequency propagation.

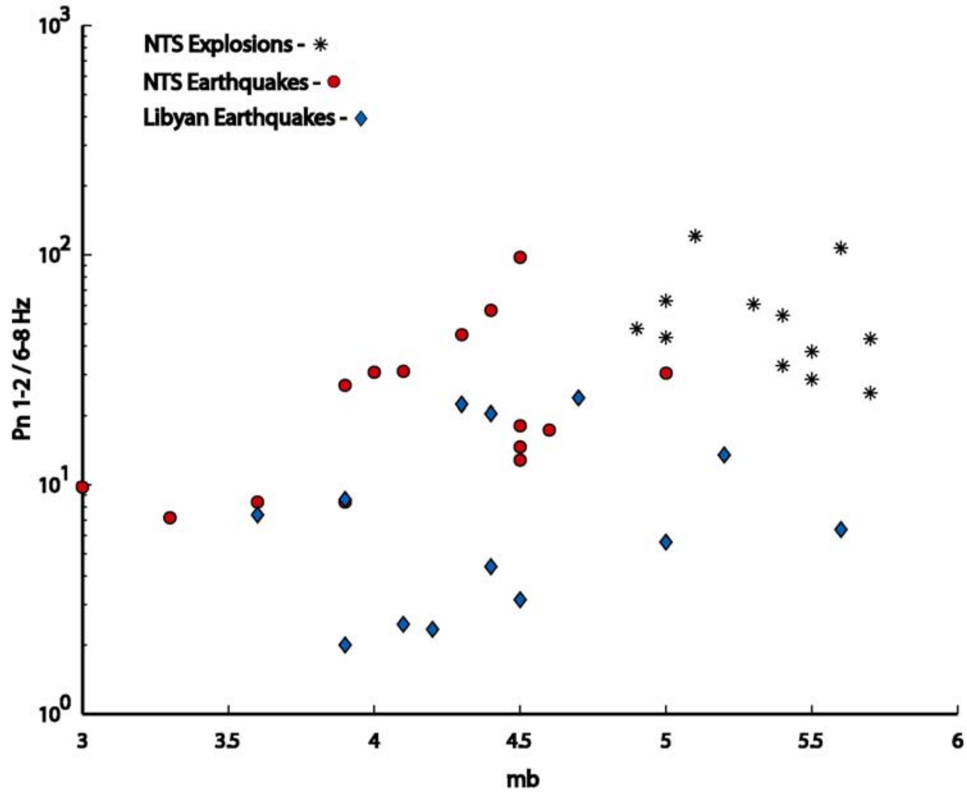

Figure 9: Cross-Spectral ratio comparison of regional Libyan earthquakes and Nevada Test Site (NTS) explosion and earthquake events. All Libyan events were recorded at KEG; note the good separation of the Libyan and NTS populations through the entire magnitude range.

CONCLUSIONS AND RECOMMENDATIONS

Our average 1-D velocity model for Libya worked well in predicting the *P*-wave arrival time for seismic events, but could not produce surface wave synthetics that matched the seismic data at frequencies less than 20 s. This could be due to the fact that we are close to the plate margin and an average 1-D velocity model may not work suitably because of the thinning of the crust. We obtained better results when we developed path specific 1-D velocity models (1.5D approach). In this case, there was a significant increase in the correlation of the synthetic seismogram and the data. At this stage, we do not have enough data to completely validate our model, but as more events occur with a significant portion of the source receiver path traversing Libya, we expect to further update and test LIBYA3D.

For regional station KEG, we see a strong correlation between percentage of continental crust and signal propagation in the high frequency ranges; however, this relationship does not persist for IDI, WDD, and TAM, where there is a lack of data. Most of the paths for IDI and WDD are purely oceanic, since they are island stations, while the paths for TAM are purely continental, which skews the results. We feel that given a full range of data that this parameter will consistently predict high frequency propagation events that would aid in verification work in regions of mixed crusts. Using LIBYA3D, we found weak correlations for all four stations when comparing crustal volumes to cross-spectral values. We feel more data is needed before drawing any solid conclusions on the relationship between crustal volume and high frequency propagation.

REFERENCES

Carmicheal R. S., 1989, Practical handbook of Physical Properties of Rocks and Minerals, CRC Press, Inc. 2000, 741 pp.

Dial, P., 1998, An integrated geophysical study of North Africa and Mediterranean lithospheric structure, *PhD. Dissertation,* University of Texas at El Paso 207 pp.

Goudarzi, G.H, and Smith J.P., 1978, Preliminary-structure contour map of the Libyan Arab Republic and other adjacent areas, *USGS.*

Hearn, P. Jr., et Al, 2001, Global GIS Database: Digital Atlas of Africa, *USGS. Digital Data Series (DDS-62-B).*

McNamara, D.E., Walter, W.R., Shultz, C. and Goldstein P., 1996, Regional phase propagation in northern Africa and the Mediterranean (abstract), *Seism. Res. Lett.,* 67, p 47.

Nafe, J.E. & Drake, C.L., 1957. Variation with depth in shallow and deep water marine sediment of porosity, density and the velocities of compressional and shear waves, *Geophysics*, 22, 523-553.

Seber, D.E., Sandoval E., Vallve, M., Brew, G. And Barazangi, 1996, Development of a geological and geophysical information system and seismological studies in the Middle East and north Africa, *Proceedings of the 18th Annual Seismic Research Symposium on Monitoring a CTBT*, 4-6 September 19996, pp. 1026-1035, PL-TR-96-2153, ADA313692.

Velasco, A.A., Hartse, H.E., Randall, G.E. (2003) Propagation or Source? Analysis of a Moderate-Magnitude Seismic Event in the Qinghai Province, China, *Bull. Seism. Soc. Am.* 93, 2281-2288.

Walter, W.R., Mayeda, K.M., Patton, H.J. (1995) Phase and Spectral Ratio Discrimination between NTS Earthquakes and Explosions. Part I: Empirical Observations, *Bull. Seism. Soc. Am.* 85, 1050-1067.

Zhang, T. & Lay, T. (1994) Analysis of Short-Period Regional Phase Path Effects Associated with Topography in Eurasia, *Bull. Seism. Soc. Am.* 84, 119-132.